Al_2O_3-films on Ni_3Al(111): a template for nanostructured cluster growth

To cite this article: C Becker *et al* 2002 *New J. Phys.* **4** 75

View the article online for updates and enhancements.

$\mathrm{Al_2O_3}$-films on $\mathrm{Ni_3Al(111)}$: a template for nanostructured cluster growth

C Becker[1]†, A Rosenhahn[1], A Wiltner[2], K von Bergmann[3], J Schneider[1], P Pervan[4], M Milun[4], M Kralj[4] and K Wandelt[1]

[1] Institut für Physikalische und Theoretische Chemie, Universität Bonn, Wegelerstraße 12, D-53115 Bonn, Germany
[2] Max-Planck-Institut für Plasmaphysik, Boltzmannstraße 2, 85748 Garching, Germany
[3] Institut für Angewandte Physik, Universität Hamburg, Jungiusstraße 11, 20355 Hamburg, Germany
[4] Institute of Physics, University of Zagreb, Bijenicka c.46, PO Box 304, 10000 Zagreb, Croatia
E-mail: cb@uni-bonn.de

Abstract. In scanning tunnelling microscope images of thin $\mathrm{Al_2O_3}$-films grown on $\mathrm{Ni_3Al(111)}$ at 1000 K two super-lattices with periodicities of 2.6 and 4.5 nm, respectively, can be identified. These well-ordered nanostructures can be used as nucleation centres for metal particle growth. It can be shown that both nanostructures act as a template for the fabrication of ordered assemblies of metal clusters by mere physical vapour deposition. The degree of ordering of these nanostructures is largely dependent on the metal deposited. Here we report on the growth of Cu, Ag, Au, Mn, and V clusters on the $\mathrm{Al_2O_3}$-films. The best results as far as ordering of the clusters is concerned was reached for V deposition at 550 K, which resulted in a nearly perfect hexagonal array of clusters with a spacing of 2.6 nm.

1. Introduction

The realization of ordered arrays of well-defined, equally sized (monodisperse) nanoclusters is the goal of many efforts in view of the development of new electronic and optoelectronic devices. Such cluster arrays would also be helpful for the study of the basic mechanisms

† Author to whom any correspondence should be addressed.

that determine the activity of heterogeneous catalysts. Here we report the realization of such periodic cluster arrays by mere vapour deposition. The intrinsic properties of the well-ordered hexagonal superstructure of alumina films grown on $Ni_3Al(111)$, used as a template for the deposition of various metals, appear to lead under defined experimental conditions to the sought ordered nucleation of metal clusters and the formation of monodisperse nanoclusters.

Much attention has lately been paid to the structuring of surfaces on the nanometre scale because of the unique properties of these structures and their potential use in the fabrication of nanoscale materials. A variety of methods has been successfully applied to the problem of nanofabrication such as laser-beam assisted deposition [1], deposition of colloidal particles [2], electron beam lithography [3], and atomic manipulation with the scanning tunnelling microscope (STM) [4]. While the latter two techniques share the high lateral resolution they both rely on a time consuming serial fabrication process. In this respect the former two methods are more apt for the fabrication of nanostructured surfaces; however, they are limited to lateral dimensions larger than 10 nm.

All these methods involve direct instrumental manipulations and are less dependent on the specific physical properties of the substrate. In contrast, a different approach has been recently proposed in which the intrinsic properties of the substrate are exploited in order to produce nanoscale structures. Strain–relief patterns and misfit dislocations of the substrate surface have been used to nucleate metallic nanostructures [5, 6] and Ge islands [7], respectively. The specific structures of the substrate used as a template for physical vapour deposition (PVD) lead to the formation of nanostructured arrays. This approach has the potential to achieve well-ordered nanoscale arrays in a single run by a self-organized process. Relying on specific properties of the substrate it is, of course, limited to a certain choice of materials.

In the present investigation we show that this approach is also applicable to the growth of ordered nanoscale arrays of metal clusters on oxide surfaces: here, in particular, thin alumina films on $Ni_3Al(111)$. This opens up a pathway to a novel strategy for the control of cluster nucleation.

Since the substrate is the determining factor we will discuss its properties first in some detail. The growth of well-ordered alumina films has been the subject of a large number of investigations [8]. These studies have shown that, in order to grow such films of high structural quality with a low density of defects, temperatures above 1000 K are needed. This high temperature excludes the direct oxidation of aluminium due to its low melting point. Instead, Ni/Al alloys have been employed by a number of research groups since they possess high melting points and the Al needed for the film growth is supplied by segregation from the bulk at elevated temperature. It is, for instance, well established that the oxidation of the NiAl(110) surface at temperatures above 1000 K leads to an Al_2O_3 film of 0.5 nm thickness [9]. On this film, however, the nucleation is either dominated by structural domain boundaries at higher temperatures (300 K) or by point defects at low temperatures (100 K) [9].

Unlike the Al_2O_3 overlayers on NiAl(110) the oxidation of a $Ni_3Al(111)$ surface at 1050 K leads to the formation of extremely homogeneous and defect-free Al_2O_3 films [10, 11]. STM images of these latter films exhibit two nanoscopic superstructures [11]. The emergence of the superstructures in the STM images is closely related to the electronic band structure of the film [12]. Just at the lower edge of the Al_2O_3 conduction band (at an STM bias voltage of $U_B = +2.3$ V) a hexagonal dot pattern with a lattice constant of 4.5 nm is

visible in the STM images. This pattern, hitherto called 'dot structure', changes into a 2.6 nm structure of hexagonal symmetry ('network structure') if the tunnelling proceeds into the conduction band of the alumina film at a sample bias above $U_B = +3.2$ V. There exists a $(\sqrt{3} \times \sqrt{3})\mathrm{R}30°$ relation between the 'network structure' and the 'dot structure' [11]. The origin of the two superstructures has not been fully explained yet but it can be shown that it is related to the lattice mismatch of the substrate ($a_s = 0.254$ nm) and the oxide film ($a_{ox} = 0.304$ nm). The strong bias dependence of the structures in the STM images suggests that the electronic properties of the film are periodically modulated. In this work we will present results that show that both the 'dot' and the 'network structure' can act as a template for the nanostructured growth of metal particles on the oxide film.

2. Experimental details

All experiments were conducted in an ultrahigh vacuum (UHV) system equipped with a STM, an Auger electron spectrometer (AES), a quadrupole mass spectrometer (QMS), and a vibrating capacitor Kelvin probe for work function change measurements. The base pressure of the UHV system was below 2×10^{-8} Pa. A $Ni_3Al(111)$ single crystal (MaTeck, Jülich) with a diameter of 7 mm and a thickness of 2 mm was used which was oriented within $0.5°$ of the (111) direction. The sample was cleaned by repeated cycles of Ar^+ ion sputtering (2.5 keV, 7.8 $\mu A\ cm^{-2}$) and subsequent annealing for 7 min at 1150 and 1000 K. The temperature of the sample could be varied between room temperature and 1400 K by direct heating monitored by a type K thermocouple which was spot-welded into a small hole on one side of the crystal. The cleanliness and composition of the thus-prepared $Ni_3Al(111)$ surface was monitored by AES.

The oxide film was prepared by exposing the sample surface to 50 L oxygen (99.998% purity, Linde) at a sample temperature of 1000 K and an oxygen partial pressure of 2×10^{-6} Pa. Following the oxygen exposure the temperature of the sample was raised to 1050 K for 5–7 min. The quality of the oxide film was then analysed with STM at room temperature. If necessary the oxidation procedure was repeated until a closed and well-ordered oxide film was obtained.

All metals were deposited by PVD. Cu, Ag, and Au were evaporated from an open tungsten basket. For Mn a Knudsen cell with an alumina crucible was used. In the case of V a rod was used, which was heated by electron bombardment. During deposition the pressure in the UHV system was in the 10^{-8} Pa range. Only in the case of V did a stronger pressure increase occur, which, however, did not apparently influence the quality of the deposited structures. Since not all the evaporators were calibrated, the amount of the deposited metal was determined from the STM images.

3. Results

One of the problems encountered when imaging clusters on oxide films is that the apparent structure of the film itself in the STM images is strongly bias dependent. Hence, favoured imaging conditions for the detection and identification of the clusters have to be established.
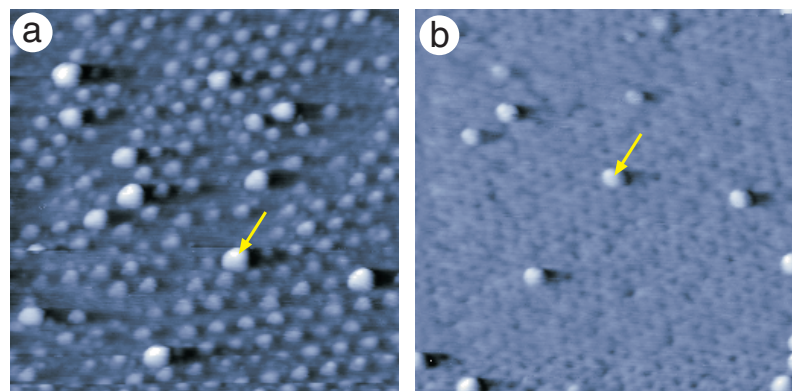
Figure 1. STM images of Ag clusters on $Al_2O_3/Ni_3Al(111)$. The images were taken at approximately the same position of the sample with different bias voltages ((a): $U_b = 2.1$ V, (b): $U_b = 3.2$ V). The tunnelling current was $I_t = 100$ pA in both cases. The image size is 60 nm $\times$ 60 nm.

The situation is depicted in figure 1. Here a small amount of Ag was deposited. Figure 1(a) shows the resulting STM image for a bias voltage of $U_b = 2.1$ V. Under these imaging conditions both the clusters and the 'dot structure' appear as protrusions. Some of these protrusions appear bigger than others suggesting that they are caused by clusters. The situation can be clarified by looking at the image b, which has been acquired at a bias voltage of $U_b = 3.2$ V. In this case the 'network structure' is visible, only the clusters are imaged as protrusions. The yellow arrow in both images marks the same cluster. This example proves that the big protrusions in figure 1(a) are clearly caused by clusters. Furthermore, the images show that different bias voltages should be used for different purposes. In order to unambiguously identify clusters, either low ($U_b \approx 0.7$ V, see figure 4(a)) or high bias voltages ($U_b > 3.0$ V) should be used. To establish the geometrical relation between the 'dot structure' and the clusters the bias voltage should be in the range of 2.0 V $< U_b < 2.8$ V where both the clusters and the 'dot structure' are visible.

The first metal we used for cluster growth was Ag, the reason being that Ag is used in industry as the prime ethene epoxidation catalyst [15]. Figure 1(a) shows the situation for a small coverage of Ag, which was deposited at room temperature. It is clearly visible that the Ag forms clusters and the clusters grow exclusively on sites of the 'dot structure'. Apparently, the protrusions that form the 'dot structure' act as nucleation centres for the cluster growth. This situation, however, changes when larger amounts of silver are deposited (figure 2). Under these conditions, rather large agglomerates of Ag are formed, the size of these exceeding the lattice constant of the 'dot structure' (4.5 nm). Hence, no correlation between the Ag aggregates and the oxide structure exists. This suggests that in this case the mutual Ag–Ag interaction exceeds the Ag–oxide interaction favouring the formation of larger Ag islands. An indication of the weak Ag–oxide interaction is also given by the existence of Ag islands with sharp lower edges (arrows). Here the STM tip has apparently carried away the lower part of the Ag islands during the scan.

Since the ultimate goal of our investigations was to generate ordered arrays of clusters we turned our interest away from Ag and decided to systematically look at the growth of the two
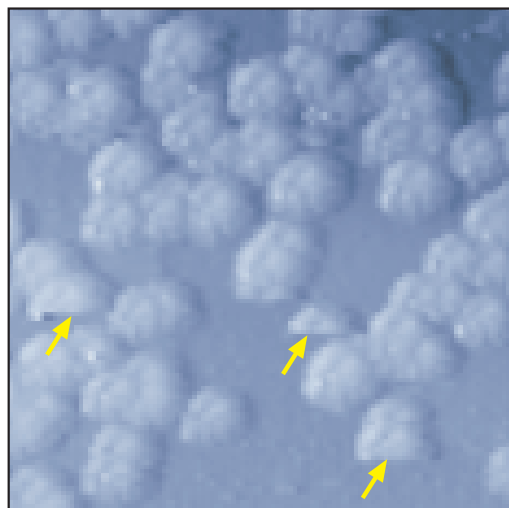
Figure 2. STM image of Ag clusters on $Al_2O_3/Ni_3Al(111)$. The bias voltage was $U_b = 0.7$ V; the tunnelling current was $I_t = 100$ pA. The image size is 80 nm $\times 80$ nm.

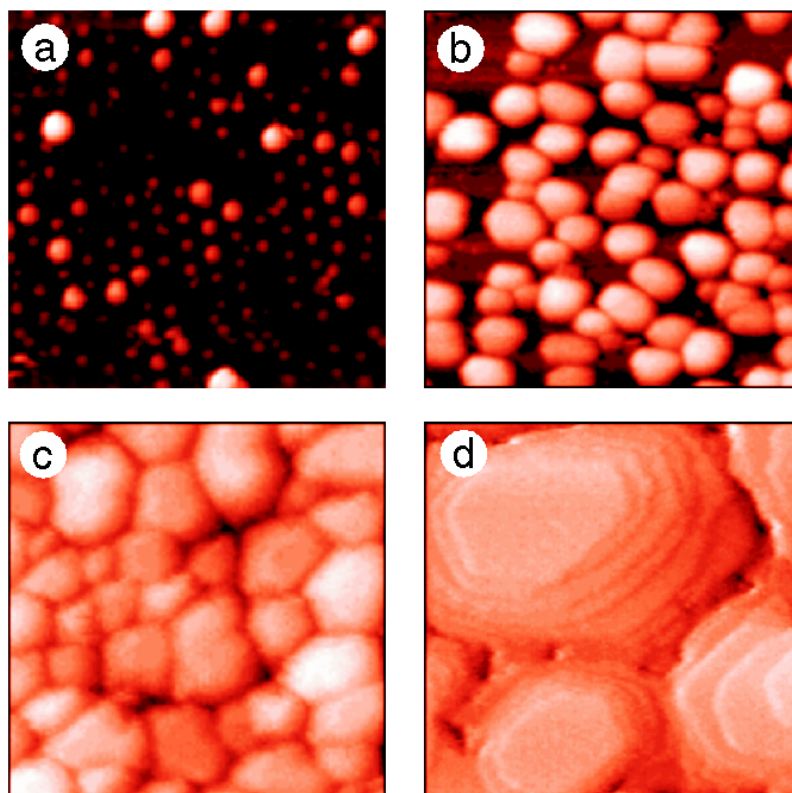**Figure 3.** STM images of Au clusters on $Al_2O_3/Ni_3Al(111)$ for different coverages. The images were taken at bias voltages of $U_b = 2.1$ V (a) and $U_b = 0.7$ V (b)–(d), respectively. The tunnelling current was $I_t = 100$ pA in all images. The image size is 60 nm $\times 60$ nm for all images.
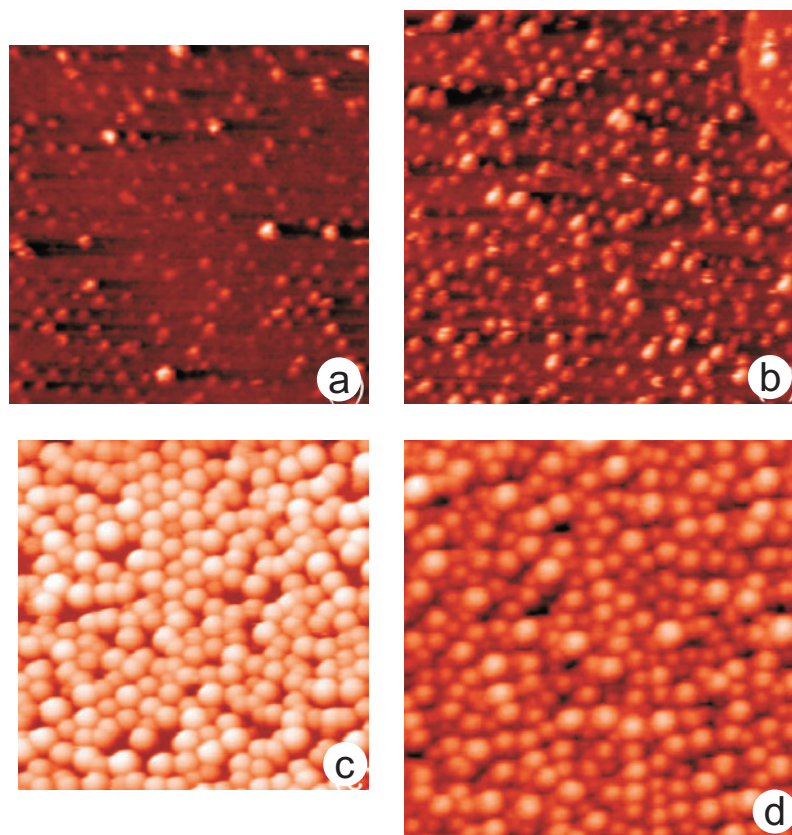
Figure 4. STM images of Cu clusters on $Al_2O_3/Ni_3Al(111)$ for different coverages. The images were taken at bias voltages of $U_b = 2.1$ V (a) and $U_b = 0.7$ V (b)–(d), respectively. The tunnelling current was $I_t = 110$ pA (a), (c) and $I_t = 120$ pA (b), (d). The image size of (a) is 72 nm $\times$ 72 nm. The other images have been scaled accordingly.

other noble metals Au and Cu. In figure 3 the growth of Au on $Al_2O_3/Ni_3Al(111)$ is depicted. The situation for low Au coverage deposited at room temperature (figure 3(a)) is similar to that at low Ag coverage. Again, quite a few Au clusters can be identified. All these clusters sit on the 'dot structure' indicating that, as in the case of Ag, nucleation preferentially takes place on this structure. At higher Au coverage this effect is, however, again dominated by the creation of larger Au aggregates (figure 3(b)). Further increase of the amount of deposited Au leads to the growth of granular films (figure 3(c)) and eventually to closed Au films with rather large islands (figure 3(d)). Again the Au–Au interaction obviously surmounts the Au–oxide interaction.

To complete the series of noble metals Cu was deposited at room temperature. As in the case of Ag and Au an initial nucleation on the 'dot structure' is found (figure 4(a)) proving that the growth is indeed governed by the protrusions of the dot structure. Unlike for the two other noble metals, however, this selective growth on the 'dot structure' persists for higher coverage (figure 4(b)). In figure 4(c) a clear indication for well-ordered cluster growth is visible. In several parts of the STM image well-ordered hexagonal arrays of Cu clusters are present. At even higher
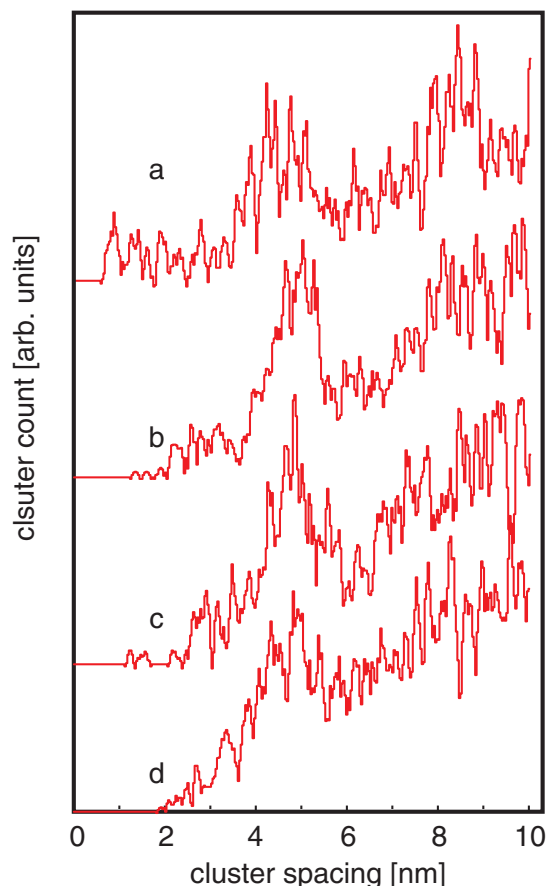
Figure 5. Radial distribution functions calculated from the STM images in figure 4. The lettering of the curves reflects the lettering of the STM images.

Cu coverage this order is, however, partially lost, but the clusters, unlike as for Ag and Au, stay rather small and do not form large aggregates (figure 4(d)). The remarkable degree of order that is reached for Cu clusters can also be seen in the radial distribution functions of the clusters in figure 5. These were calculated for the STM images in figure 4 by analysing the distance from the centre of each individual cluster to the centres of all other clusters. Clearly, a peak around 4.5 nm can be seen in the radial distribution function corresponding to the nearest-neighbour distance for the clusters. Since this value is also equal to the lattice constant of the 'dot structure', this again proves that the 'dot structure' acts as template for the cluster growth providing an ordered array of nucleation centres. From the absence of any longer range peaks in the radial distribution functions it can be concluded that in the case of Cu clusters order is a local phenomenon. It can be inferred that the reason for the higher order in the $Cu/Al_2O_3/Ni_3Al(111)$ systems compared to the other noble metals is related to the stronger Cu–oxide interaction. We will address this point in section 4.

Based on these findings we turned our attention to two metals, which possess an even stronger metal–oxide interaction: Mn and V. For Mn again the room temperature deposition was studied. The results are depicted in figure 6. For low coverage (figure 6(a)) apparently a similar situation as for Ag, Au, and Cu is encountered. The clusters show a certain tendency for
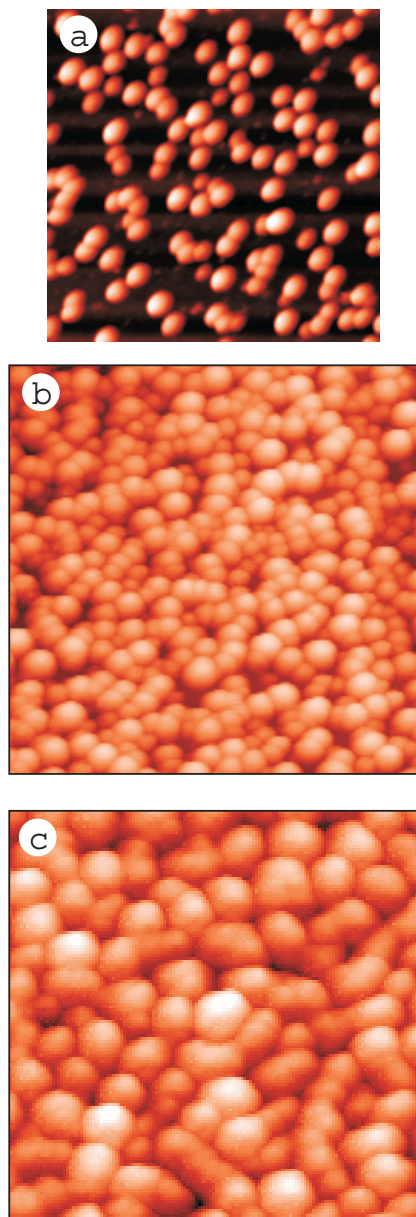
Figure 6. STM images of Mn clusters on $Al_2O_3/Ni_3Al(111)$ for different coverages. The images were taken at bias voltages of $U_b = 0.7$ V. The tunnelling current was $I_t = 330$ pA. The image size of (a) is 65 nm × 65 nm. The other images have been scaled accordingly.

ordering and hexagonal arrangements of Mn clusters are visible in the image. However, if we analyse the images more closely a new feature becomes visible. The radial distribution function in figure 7(a) shows not only the expected peak at 4.5 nm corresponding to the 'dot structure', but also a peak at 2.6 nm, which can be related to the 'network structure'. This is a new feature, indicating that in the case of Mn not only the 'dot structure' but also the 'network structure' acts as a nucleation centre. This situation persists at higher Mn coverage (figure 6(b)) where
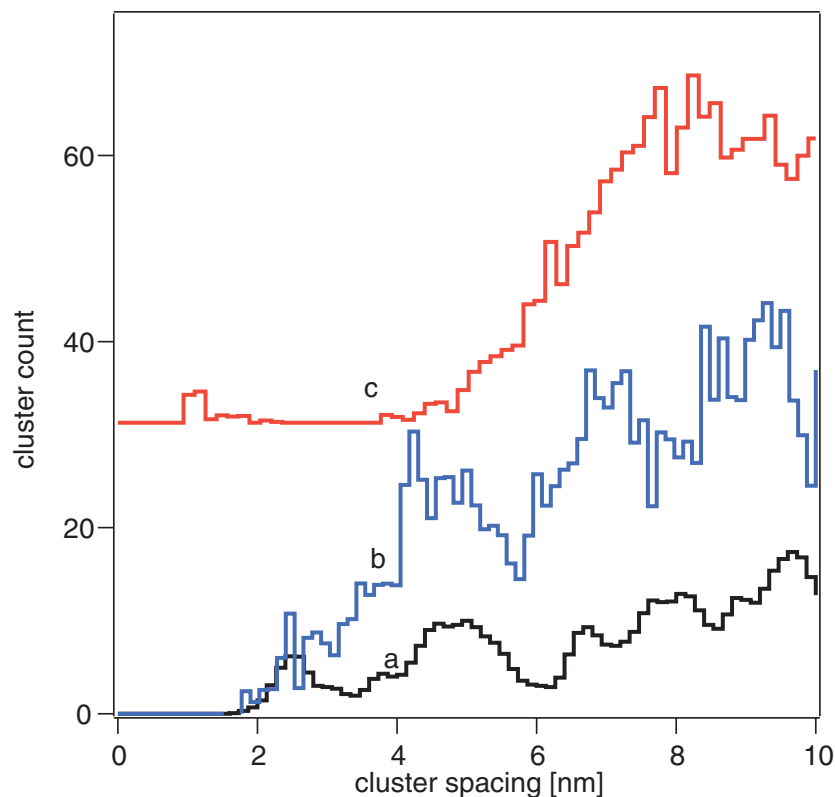
Figure 7. Radial distribution functions calculated from the STM images in figure 6. The lettering of the curves reflects the lettering of the STM images.

clusters grow on both the 'network' and the 'dot structure'. However, the peak around 2.6 nm is now smaller in relation to that at 4.5 nm, indicating that a preference for the 'dot structure' still exists (figure 7(b)). Only at very high Mn coverage is the order lost, and large Mn particles are formed (figure 6(c)). This is also visible in the radial distribution function (figure 7(c)) where a first maximum appears around 8 nm, which reflects the average size of the Mn clusters in the image.

Finally, the growth of V at room temperature has been investigated. In figure 8, a series of STM images for different V coverages is shown. It can be seen that, beginning at low coverage, the growth is relatively well ordered. However, the size distribution of the clusters is not very uniform. This behaviour persists even at higher coverage (figures 8(b) and (c)). The corresponding radial distribution functions in figure 9, however, indicate a high degree of spatial order for the two highest coverages. Clear maxima can be seen around 2.6 and 4.5 nm. This has led us to the conclusion that the formation of small clusters is favoured. Accordingly the substrate temperature during growth was increased in order to facilitate the diffusion of V. The result of these experiments is shown in figure 10. At a substrate temperature of 550 K a nearly perfect hexagonal array of V clusters is obtained (figure 10(a)). From this STM image an autocorrelation image was calculated (figure 10(b)). The hexagonal order of the cluster array is clearly visible. Furthermore, the high degree of spatial order is reflected by the fact that the hexagonal order extends over a long range in the autocorrelation image. Closer inspection of the structure reveals that V prefers to grow on the 'network structure'. This immediately becomes
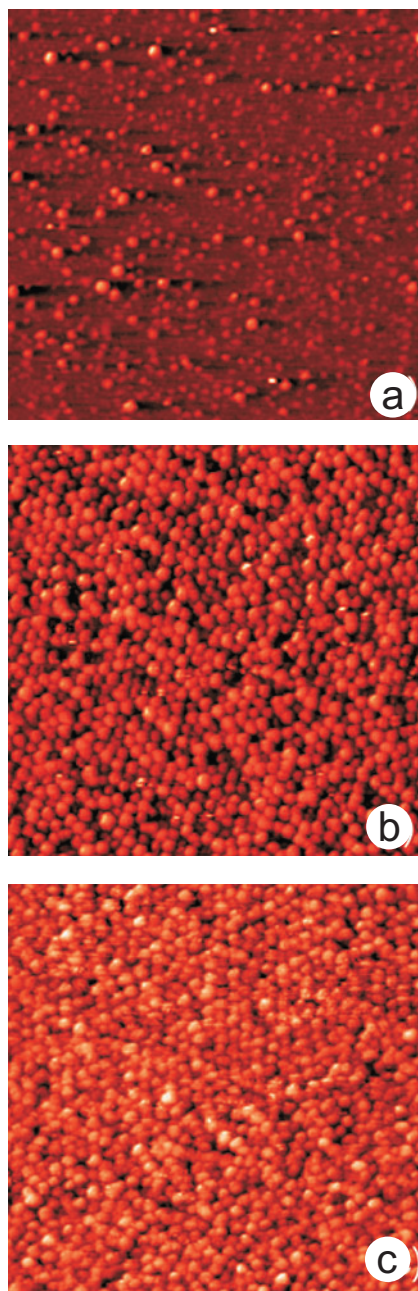
Figure 8. STM images of V clusters on $Al_2O_3/Ni_3Al(111)$ for different coverages. The images were taken at bias voltages of $U_b = 0.7$ V. The tunnelling current was $I_t = 110$ pA. The image size is 80 nm $\times$ 80 nm.

obvious in figure 11 where the radial distribution function of the STM image in figure 10 is compared to the radial distribution function of the network structure. This is a surprising result since all other metals had a preference for growing on the 'dot structure'. However, in the case of Mn a small deviation from this behaviour has already been found. We discuss possible reasons for this change of behaviour in the following section.
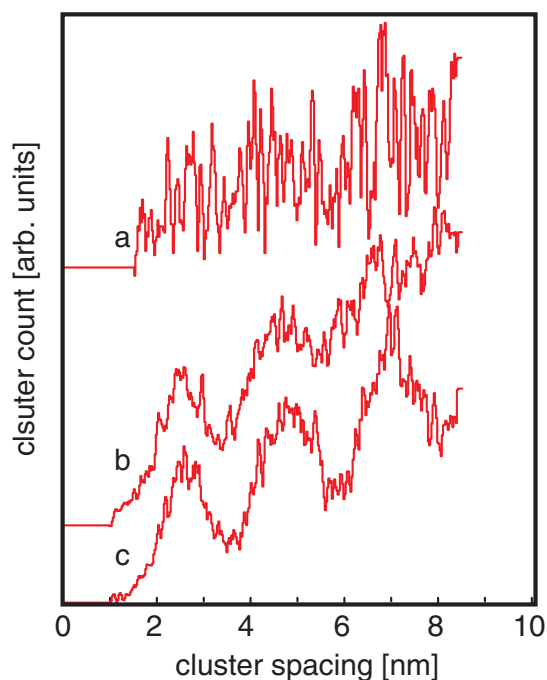
Figure 9. Radial distribution functions calculated from the STM images in figure 8. The lettering of the curves reflects the lettering of the STM images.
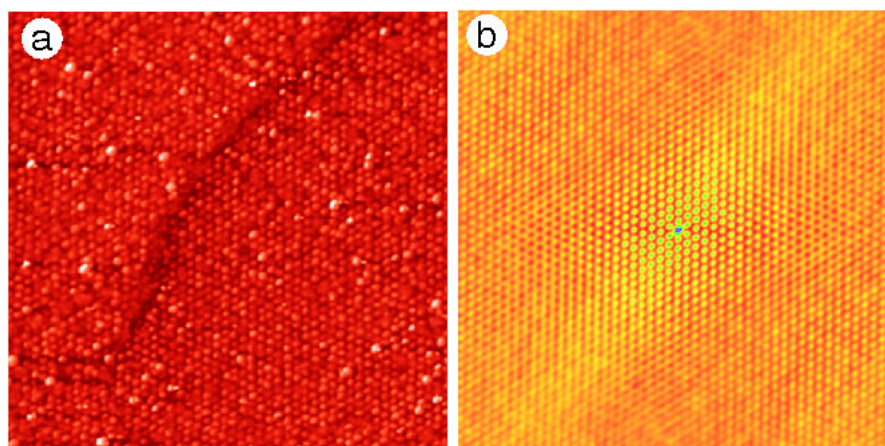

Figure 10. (a): STM image of V clusters on $Al_2O_3/Ni_3Al(111)$ grown at a substrate temperature of $T_{sub} = 550$ K. The image was taken at a bias voltage of $U_b = 0.7$ V. The tunnelling current was $I_t = 100$ pA in both cases. The image size is $125\,\text{nm} \times 125\,\text{nm}$. Image (b) shows the autocorrelation image calculated from (a).

4. Discussion

A first indication about the metal–oxide interaction strength can be derived from the heat of formation of the respective metal–oxide species. An overview of these values is given in table 1.
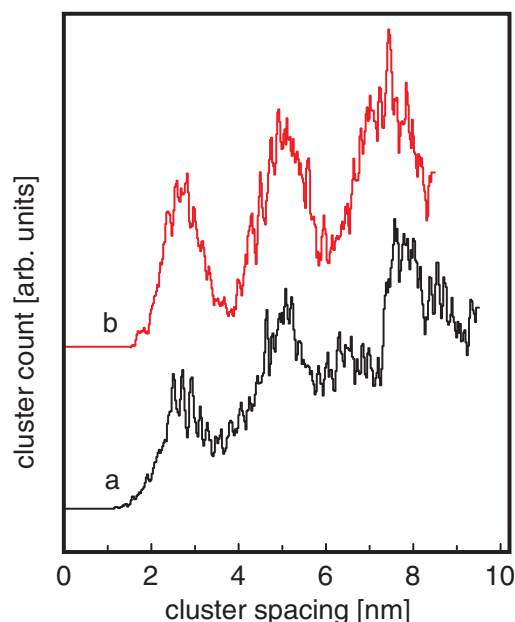
Figure 11. Radial distribution functions of the 'network structure' of the alumina film (curve a) and of the clusters in figure 10 (curve b).

Table 1. Heats of formation referred to one mole of atomic oxygen of various metal–oxides. Adhesion energies E_{adh} of various metals on alumina [17]. Cohesive energies E_{coh} of the same metals.

Metal	$-\Delta_f H^0$ (kJ mol^{-1})	E_{adh} (mJ m^{-2})	E_{coh} (kJ mol^{-1})
Au	< 0 [16]	265	379
Ag	31 [18]	323	285
Cu	157, 169 [18]	490	337
Mn	260, 385 [18]	863, 1285	282
V	310, 432 [18]	—	512
Al	559 [18]	—	—

The first obvious conclusion is that for all metals employed in this study the heat of formation $\Delta_f H^0$ of the respective oxide is smaller than that of Al_2O_3. This indicates that a reduction of the alumina film by the deposited metal is not likely at the low temperatures applied during growth. Furthermore, the adhesive energies E_{adh} show qualitatively the same behaviour as the heat of formation indicating that the interaction strength between metal and alumina film increases in this series from Au to V.

The first observation concerning the nucleation and the growth of the particles on the alumina film is that at low coverage all metals used in this study show a strong preference for nucleation on the 'dot structure', a fact which can be related to the 'dot structure' as providing the nucleation centres, which has already been demonstrated for Mn clusters on these films [13]. Apparently this structure provides nucleation sites for clusters very much like defects on, for example, MgO [14], suggesting that heterogeneous nucleation governs the growth.
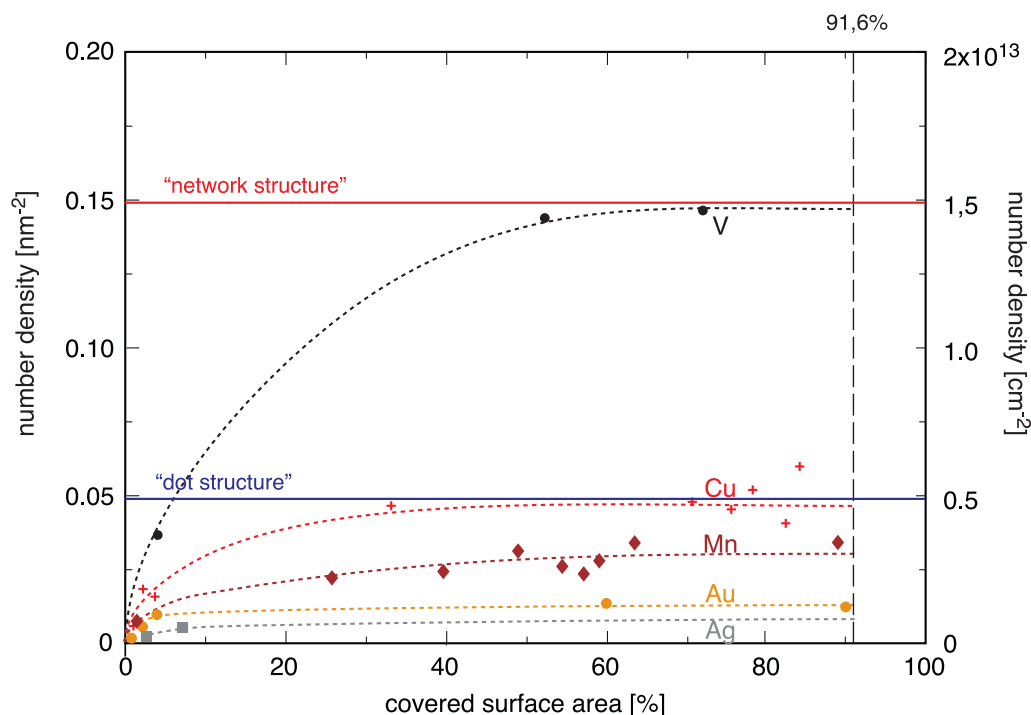
Figure 12. Number densities of the clusters as a function of covered surface area. The covered surface area was calculated from the ratio of surface area covered by clusters and the total surface area of the respective STM image. The value 91.6% corresponds to a hexagonal close-packed array of spherical particles. The number densities of equivalent sites of the 'dot' (blue line) and the 'network structure' (red line) are also shown.

This leads to the question of whether the further cluster growth is thermodynamically or kinetically controlled. In the high-coverage regime the growth behaviour becomes distinct for all the different metals. This is summarized in figure 12 where the number density of clusters is displayed as a function of occupied surface area. Here the number density reaches a distinct value for the each metal. Not surprisingly, the values reached for V and Cu clusters—the metals for which the highest order of the cluster arrays was obtained—correspond roughly to the number densities calculated for sites of the 'network' and the 'dot structure', respectively.

However, the general ranking of the metals is neither in line with the strength of the metal–oxide interaction strength nor with the adhesive and cohesive energies. In particular, for Mn a much lower number density is obtained than for V even though the interaction strength of Mn is comparable to that of V. This behaviour can be qualitatively understood if we take a look at the cohesive energies of these metals (table 1). Since the metal–oxide interaction for V and Mn is roughly of equal strength the cohesive energy of the metal itself should play a crucial role. Indeed, we see that the cohesive energy of manganese is much smaller than that of V. Accordingly, the tendency for forming small particles at the expense of contact area between metal and oxide will be smaller for Mn than for V. This will ultimately lead to larger Mn particles at high coverage, as is observed in the STM images.

In general, one could argue that metals with higher cohesive energies tend to form smaller particles thus yielding ordered cluster arrays. This would also apply to Cu, which indeed shows this behaviour, but also to Au. In the latter case the small adhesive energy should even favour the growth of particles. Instead, growth of granular films and eventually rather smooth films is observed. We, therefore, concluded that the most important fact for the generation of ordered cluster arrays, besides the presence of appropriate nucleation centres, is growth kinetics. This has been demonstrated for V where the increase of the substrate temperature to 550 K during growth yielded almost perfectly ordered cluster arrays.

The question concerning the kinetics of the growth process of clusters becomes even more pending when one considers recent results by Carrey *et al* [19] on the mobility of small Au particles on amorphous alumina. They were able to show that defects of the alumina act as nucleation centres, but that above a critical size the thus-formed clusters detach again and become mobile. This result suggests that the growth of the clusters may, indeed, be more complex than we used to think. Thus, not only the macroscopic parameters of the growth process such as impinging metal flux and substrate temperature have to be considered, but also the microscopic details, such as mobility of metal atoms and clusters as well as stability of nucleation centres as a function of cluster size. This calls for experiments at low temperature where these parameters are directly accessible by STM.

5. Conclusion

The room temperature growth of Au, Ag, Cu, Mn, and V clusters on thin alumina films on $Ni_3Al(111)$ has been investigated by STM. It has been shown that at low coverage these metals nucleate preferentially on the nanoscopic 'dot structure', which is visible in the STM images of the oxide film. At higher coverage the growth shows big variations between the employed metals. Whereas the deposition Au, Ag, and Mn did not lead to the desired formation of ordered cluster arrays at high coverage, the growth of Cu and V at room temperature resulted in the formation of rather well-ordered cluster arrays. For V the homogeneity of the cluster array could be improved by deposition at elevated substrate temperature (550 K).

The results show that ordered arrays of metal clusters can be manufactured by mere PVD using a thin alumina film on $Ni_3Al(111)$ as a template. In this case, the nucleation of the clusters is controlled by the nanoscopic superstructures of the film; the 'dot structure' and the 'network structure', respectively.

References

[1] McClelland J J, Scholten R E, Palm E C and Celotta R J 1993 *Science* **262** 877
[2] Shipway A N, Katz E and Willner I 2000 *Chem. Phys. Chem.* **1** 18
[3] Wong K, Johansson S and Kasemo B 1996 *Faraday Discuss.* **105** 237
[4] Avouris P 1995 *Acc. Chem. Res.* **28** 95
[5] Brune H, Giovannini M, Bromann K and Kern K 1998 *Nature* **394** 451
[6] Bromann K, Giovannini M, Brune H and Kern K 1999 *Eur. Phys. J.* D **9** 25
[7] Yu S *et al* 1997 *Phys. Rev. Lett.* **78** 503
[8] Franchy R 2000 *Surf. Sci. Rep.* **38** 195
[9] Bäumer M and Freund H-J 1999 *Prog. Surf. Sci.* **61** 127

Institute *of* **Physics** Φ DEUTSCHE PHYSIKALISCHE GESELLSCHAFT

[10] Becker C, Kandler J, Raaf H, Linke R, Pelster T, Dräger M, Tanemura M and Wandelt K 1998 *J. Vac. Sci. Technol.* A **16** 1000

[11] Rosenhahn A, Schneider J, Becker C and Wandelt K 2000 *J. Vac. Sci. Technol.* A **18** 1923

[12] Rosenhahn A, Schneider J, Kandler J, Becker C and Wandelt K 1999 *Surf. Sci.* **433–435** 705

[13] Becker C, von Bergmann K, Rosenhahn A, Schneider J and Wandelt K 2001 *Surf. Sci.* **486** L443

[14] Henry C R 1998 *Surf. Sci. Rep.* **31** 231

[15] Serafin J G, Liu A C and Seyedmonir S R 1998 *J. Mol. Catal.* **131** 157

[16] Henrich V E and Cox P A 1994 *The Surface Science of Metal Oxides* (Cambridge: Cambridge University Press)

[17] Chatain D, Rivollet I and Eustathopoulos N 1986 *J. Chim. Phys.* **83** 561

[18] 2001 *Handbook of Chemistry and Physics* 81st edn (Boca Raton, FL: Chemical Rubber Company Press)

[19] Carrey J, Maurice J-L, Petroff F and Vaurès A 2002 *Surf. Sci.* **504** 75